Supporting Information

for

Fabrication of Hollow-shape CuO Nanoparticle Assembly with Sacrificial $W_{18}O_{49}$ Template for C_{2+}-Product-Selective Electrochemical CO_2 Reduction

Shan Wang†[abc], Chen Yang†[abc], Feng Chen[bd], Lin-Jun Zhu[bd], Wen-Wen Wang[bce], Qi Hong[bce], Teng Zhang*[bcd]

[a.] College of Chemistry, Fuzhou University, Fuzhou 350108, China.

[b.] State Key Laboratory of Structural Chemistry, Fujian Institute of Research on the Structure of Matter, Chinese Academy of Sciences, Fuzhou 350002, China.

[c.] Fujian College, University of the Chinese Academy of Sciences, Fuzhou 350002, China.

[d.] University of the Chinese Academy of Sciences, Beijing, 100049, China.

[e.] College of Chemistry and Materials Science, Fujian Normal University, Fuzhou 350117, China.

† These authors contribute equally.

* Corresponding Author: zhangteng@fjirsm.ac.cn

1. General Information

All chemicals are used as received from suppliers without further purification. Powder X-ray diffraction (PXRD) patterns were recorded on a Miniflex 600 diffractometer using Cu Kα radiation (λ = 0.154 nm). Scanning Electron Microscope (SEM) images were collected on an SU-8010 microscope. Transmission electron microscope (TEM) images and the EDS of samples were recorded by a FEIT 20 working at 200 kV. X-ray photoelectron spectra (XPS) spectra were recorded on an ESCALAB 250Xi spectrometer with a monochromatic Al X-ray source (1486.6 eV). N_2 adsorption-desorption isotherm and the Brunauer-Emmett-Teller (BET) surface area measurements were measured using Micromeritics ASAP 2460 instrument. The content of Cu was detected by inductively coupled plasma atomic emission spectroscopy (ICP-AES) on an Ultima 2 analyzer (Jobin Yvon).

2. Material Synthesis and Characterization

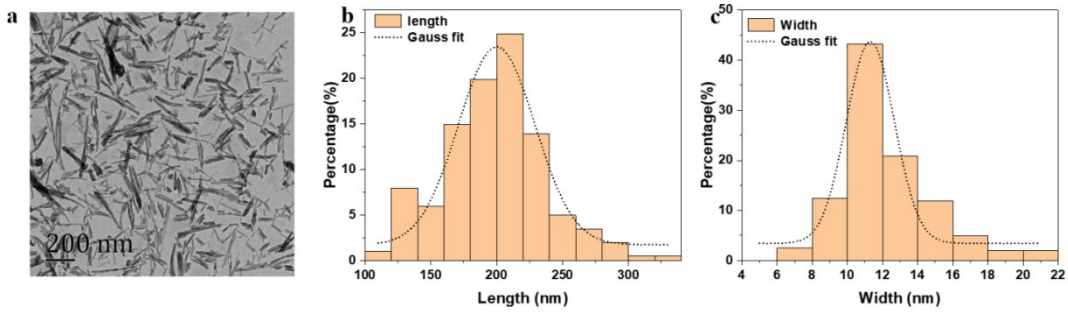

Figure S1. (a)TEM image of $W_{18}O_{49}$ nanowires; (b,c) Histograms of length (b) and width (c) distributions of $W_{18}O_{49}$ nanowires.

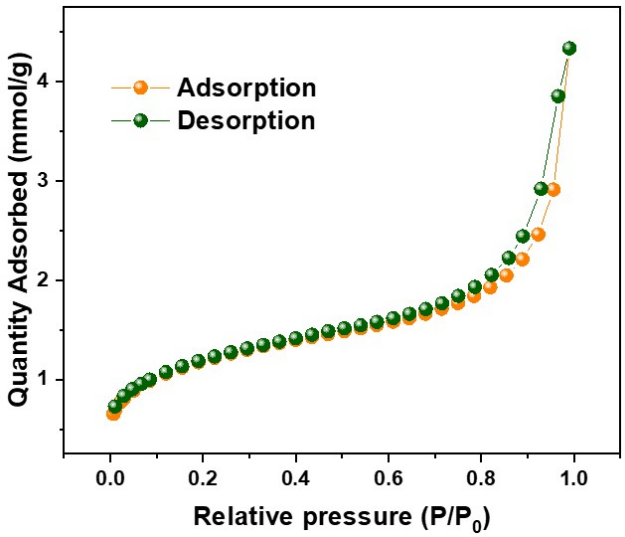

Figure S2. N_2 adsorption-desorption isotherm for $W_{18}O_{49}$.

Table S1. The synthesis conditions and Cu content in different Cu-$W_{18}O_{49}$-x samples as determined by ICP-AES.

sample	$W_{18}O_{49}$ (mg)	Na_2CO_3 (mg)	$Cu(NO_3)_2 \cdot 3H_2O$ (mg)	Cu wt.%
Cu-$W_{18}O_{49}$-0.1	100	10	10	3.33%
Cu-$W_{18}O_{49}$-0.2	100	20	20	5.11%
Cu-$W_{18}O_{49}$-0.5	100	50	50	11.84%
Cu-$W_{18}O_{49}$-1	100	100	100	27.38%
Cu-$W_{18}O_{49}$-2	100	200	200	39.06%

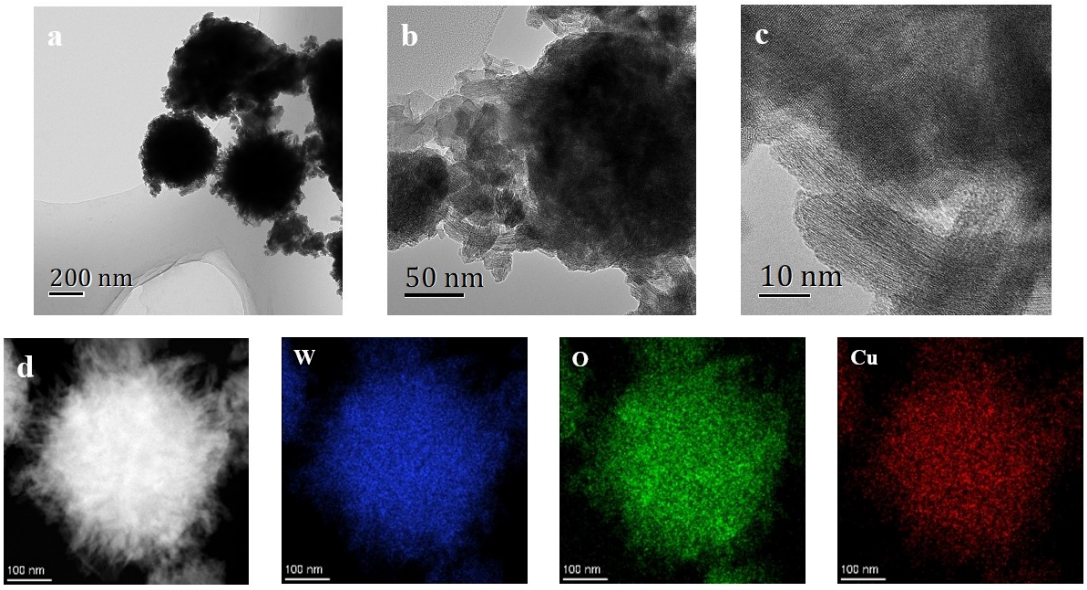

Figure S3. (a,b) TEM images of Cu-$W_{18}O_{49}$-0.1. (c) HRTEM of Cu-$W_{18}O_{49}$-0.1. (d) Energy dispersive X-ray spectroscopy (EDS) mapping images of Cu-$W_{18}O_{49}$-0.1: W (blue), O (green) and Cu (red).

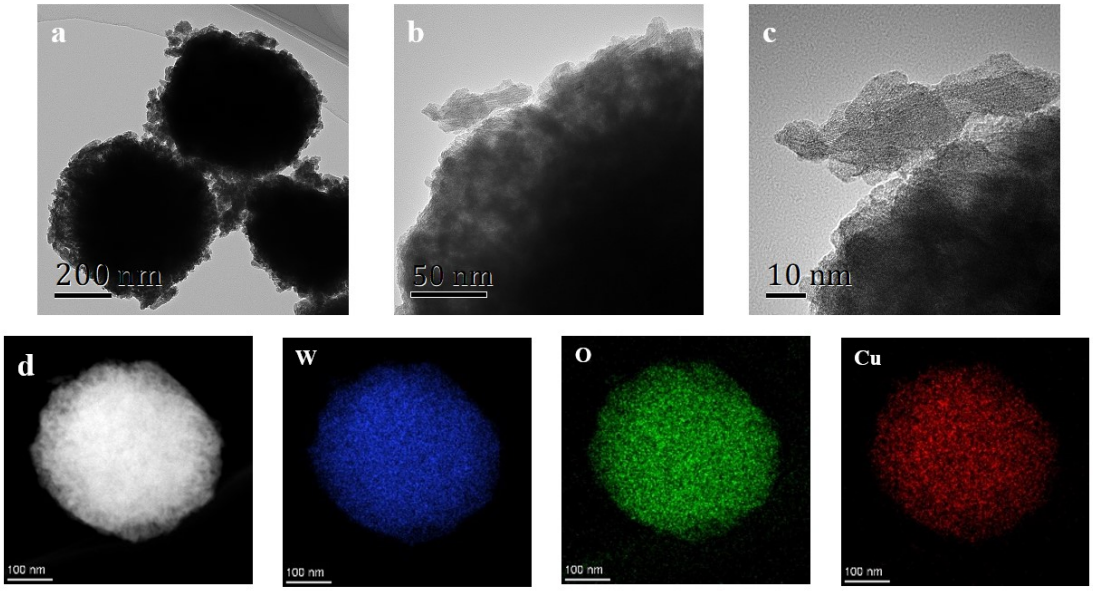

Figure S4. (a,b) TEM images of Cu-$W_{18}O_{49}$-0.2. (c) HRTEM of Cu-$W_{18}O_{49}$-0.2. (d) Energy dispersive X-ray spectroscopy (EDS) mapping images of Cu-$W_{18}O_{49}$-0.2: W (blue), O (green) and Cu (red).

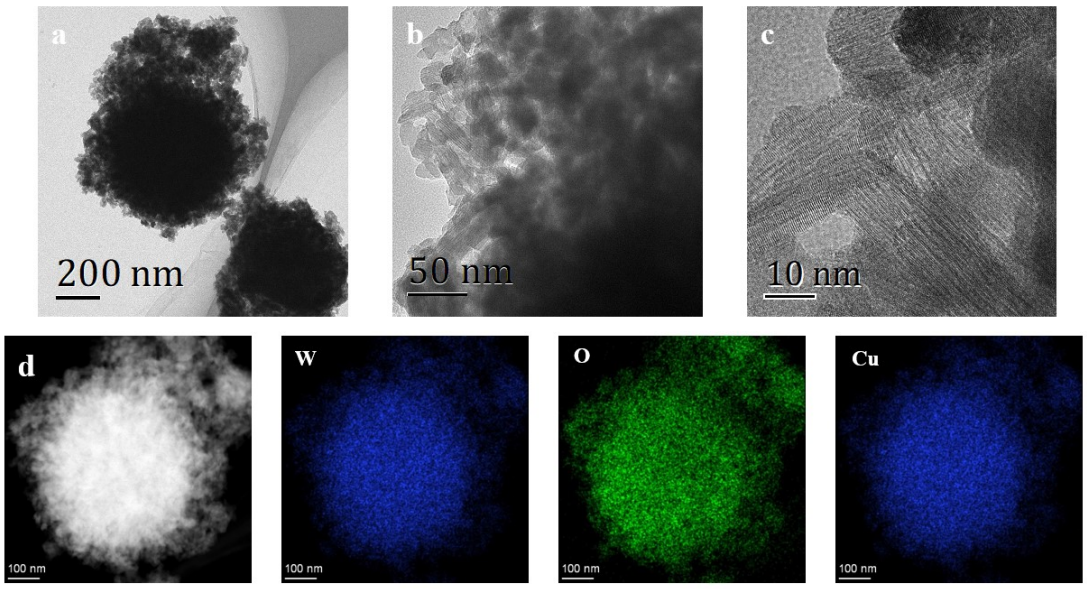

Figure S5. (a,b) TEM images of Cu-$W_{18}O_{49}$-1. (c) HRTEM of Cu-$W_{18}O_{49}$-1. (d) Energy dispersive X-ray spectroscopy (EDS) mapping images of Cu-$W_{18}O_{49}$-1: W (blue), O (green) and Cu (red).

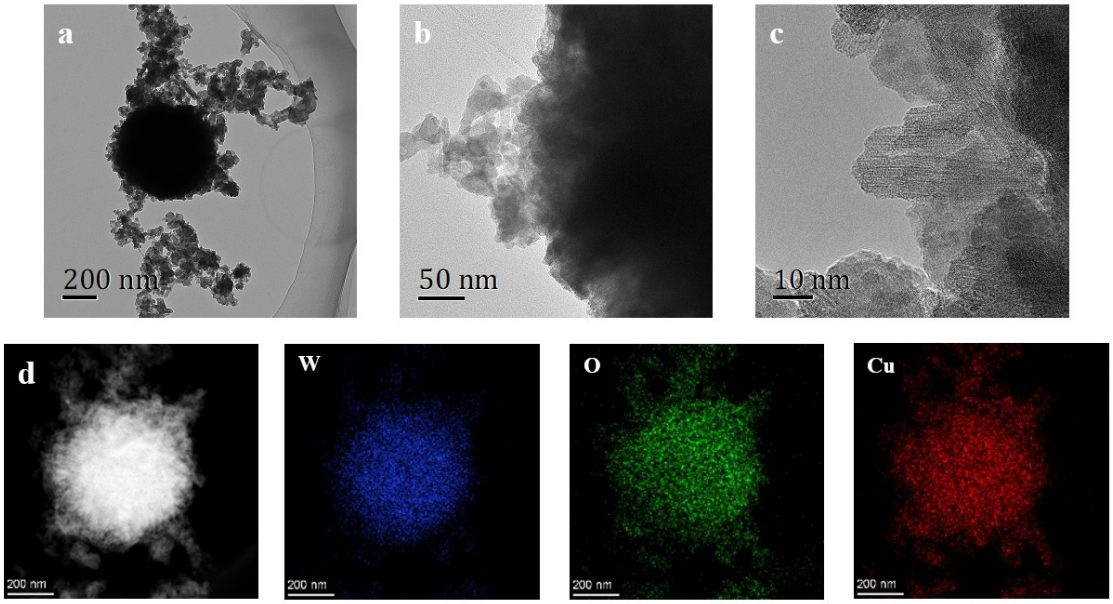

Figure S6. (a,b) TEM images of Cu-$W_{18}O_{49}$-2. (c) HRTEM of Cu-$W_{18}O_{49}$-2. (d) Energy dispersive X-ray spectroscopy (EDS) mapping images of Cu-$W_{18}O_{49}$-2: W (blue), O (green) and Cu (red).

Table S2. W 4f XPS peak fitting results of $W_{18}O_{49}$ and Cu-$W_{18}O_{49}$-x materials.

sample	W^{6+}	W^{5+}
$W_{18}O_{49}$	60.02%	39.98%
Cu- $W_{18}O_{49}$-0.2	52.65%	47.35%
Cu- $W_{18}O_{49}$-0.5	50.68%	49.32%
Cu- $W_{18}O_{49}$-1	42.72%	57.28%
Cu- $W_{18}O_{49}$-2	38.94%	61.06%

Table S3. O 1s XPS peak fitting results of $W_{18}O_{49}$ and Cu-$W_{18}O_{49}$-x materials.

sample	Adsorption oxygen (O^{ads})	oxygen defect (O^{def})	Lattice oxygen (O^{lat})
$W_{18}O_{49}$	21.27%	32.35%	46.38%
Cu- $W_{18}O_{49}$-0.2	7.94%	35.84%	56.22%
Cu- $W_{18}O_{49}$-0.5	4.63%	39.79%	55.59%
Cu- $W_{18}O_{49}$-1	6.90%	45.55%	47.55%
Cu- $W_{18}O_{49}$-2	-	52.7%	47.3%

3. X-ray Absorption Spectroscopy

The Cu K-edge XAS spectra were collected at beamline BL14W1 of Shanghai Synchrotron Radiation Facility (SSRF), China. Samples were grinded and pressed into pellets to achieve adequate absorption length. Spectra were collected in transmission mode. The X-ray beam was monochromatized by a Si(111) monochromator and detuned by 30% to minimize harmonics. The beam intensity (I_0 and I_1) was measured

by ionization chambers.

Data were processed using the Athena and Artemis programs of the Demeter package based on FEFF 6.[1, 2] Fits were performed with a *k*-weight of 3 in *R*-space. Refinement was performed by optimizing an amplitude factor S_0^2 and energy shift ΔE_0 which are common to all paths, in addition to parameters for bond length (ΔR) and Debye-Waller factor (σ^2). In order to determine the coordination number (N) of Cu in the Cu-$W_{18}O_{49}$-0.5 catalyst, the amplitude factors S_0^2 for its fit was set equal to that obtained from the fit of Cu foil standard ($S_0^2 = 0.873$).

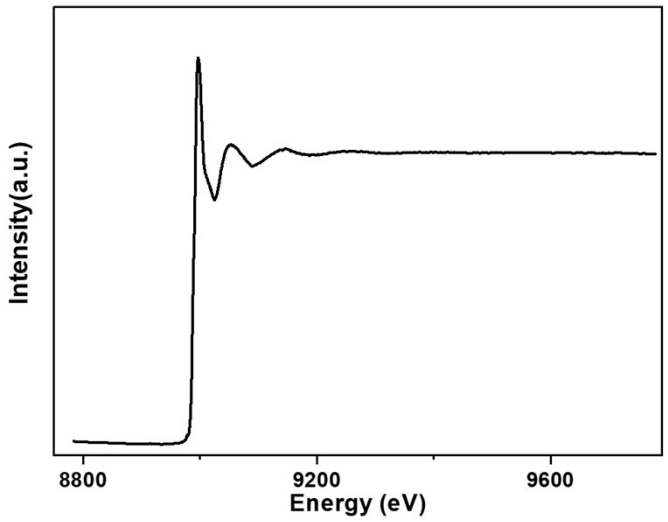

Figure S7. X-ray absorption fine structure (XAFS) characterization of Cu-$W_{18}O_{49}$-0.5.

Table S4. Summary of EXAFS fitting parameters for Cu foil standard and Cu-$W_{18}O_{49}$-0.5 catalyst.

	S_0^2	ΔE_0 / eV	scattering path	N	R / Å	σ^2 / 10^{-3} Å^2
Cu foil[a]	0.873±0.051	4.17±0.69	Cu-Cu(1)	12	2.541±0.003	8.6±0.4
			Cu-Cu(2)	6	3.88±0.01	12.0±1.4
Cu-$W_{18}O_{49}$-0.5[b]	0.873	-5.14±1.19	Cu-O	4.0±0.3	1.934±0.006	6.3±0.7

[a] Fitting range: k 3.0 – 12.486 Å^{-1}, R 1.0 – 3.5 Å; Independent points: 14.8; Number of variables: 6; R-factor: 0.4%.

[b] Fitting range: k 3.0 – 12.368 Å^{-1}, R 1.0 – 3.0 Å; Independent points: 11.6; Number of variables: 4; R-factor: 1.2%.

4. Electrochemical Studies

In control potential electrolysis experiments, the gas products were monitored by an online GC (GC9790plus, FULI Instruments) equipped with a TCD and an FID detector. H_2 was detected by TCD and other gas products were detected by FID, respectively. The liquid products were collected from the outlet of flow cell and then analyzed by ^{1}H NMR spectroscopy (600 MHz). For quantification, 500 μL of cathode electrolyte, 10 μL of internal solution (0.5 wt% DMSO in D_2O) and 100 μL of D_2O were mixed to

prepare the NMR sample. Proton chemical shifts of the liquid products are taken from previous reports.[3-5]

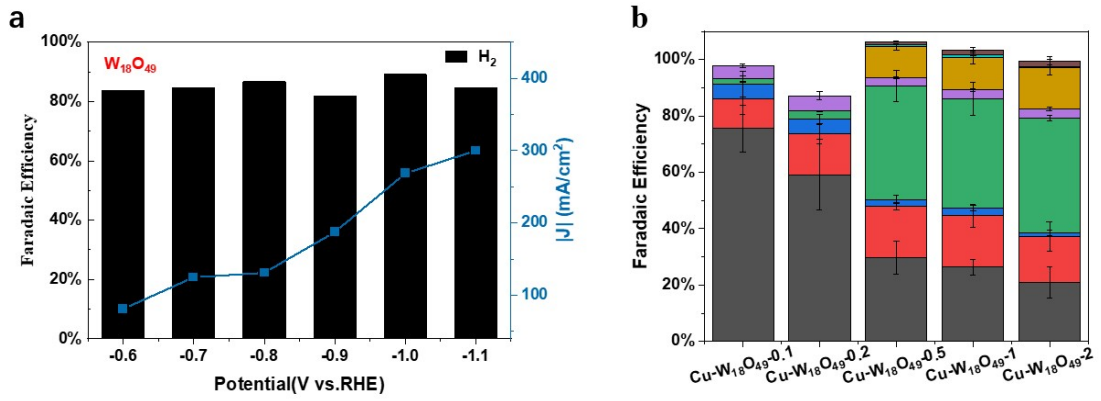

Figure S8. (a)Faradaic efficiencies (bars, left y-axis) and total current density (|j|, blue curves, right y-axis) of $W_{18}O_{49}$. (b) Faradaic efficiency comparison of samples with different Cu doping levels at -0.9 V vs RHE.

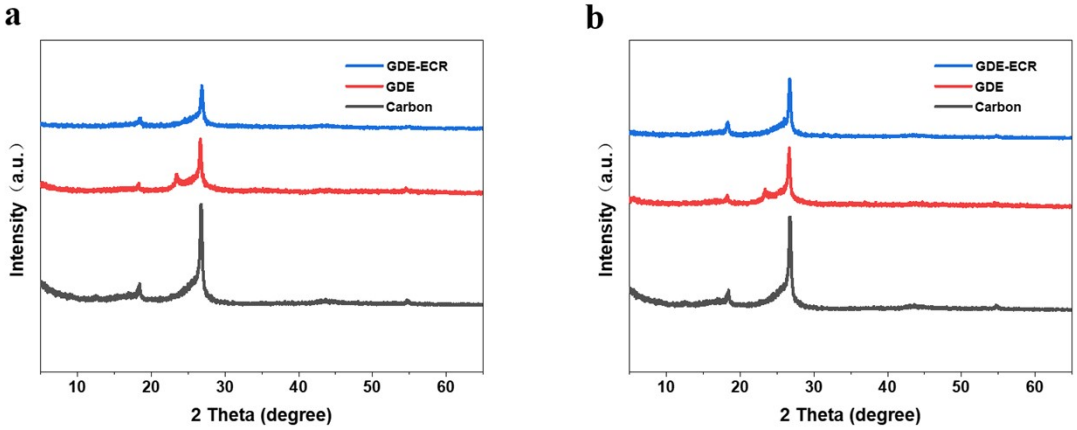

Figure S9. PXRD patterns of (a) Cu-$W_{18}O_{49}$-0.5, (b) Cu-$W_{18}O_{49}$-1 coated GDE carbon paper before and after electrolysis (-0.8 V vs RHE).

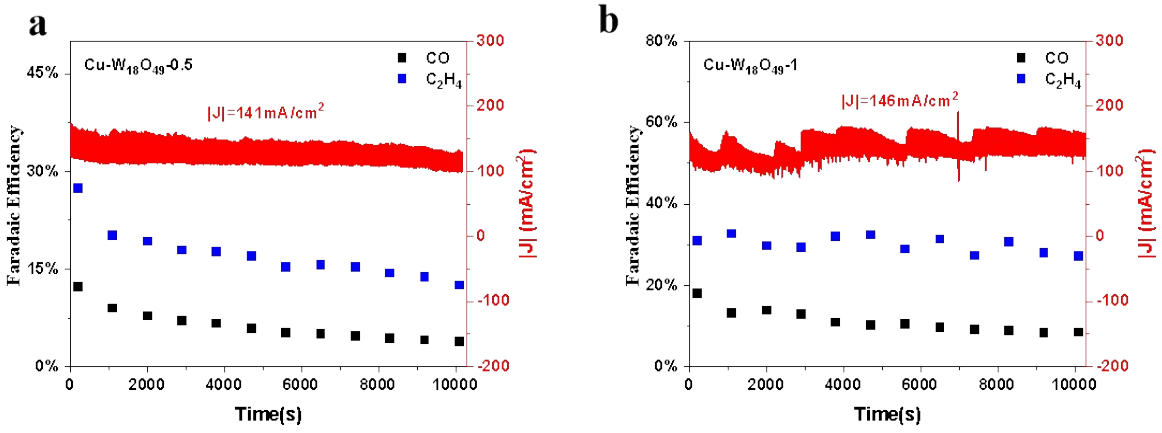

Figure S10. Long-term electrolysis performances of Cu-$W_{18}O_{49}$-0.5 (a) and Cu-$W_{18}O_{49}$-1 (b) at -0.8 V vs. RHE.

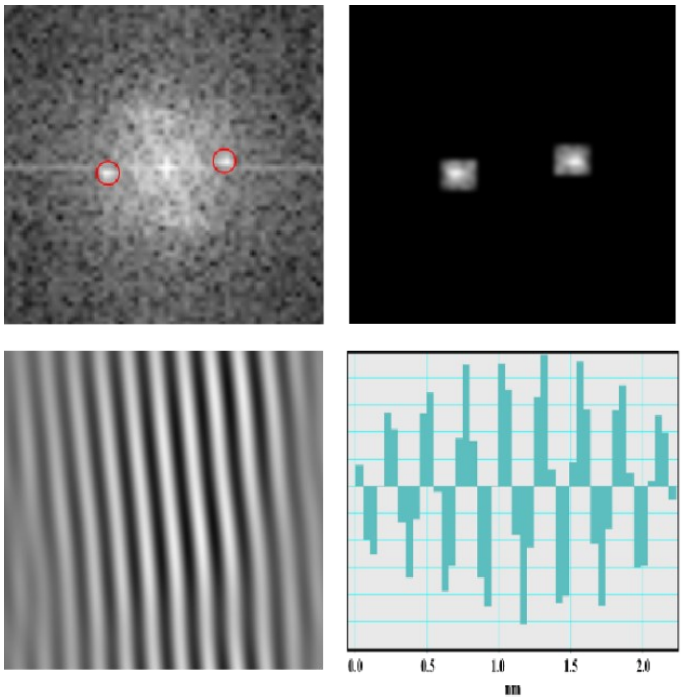

Figure S11. FFT of Cu-$W_{18}O_{49}$-0.5 material after electrolysis showing the presence of nano size CuO particles.

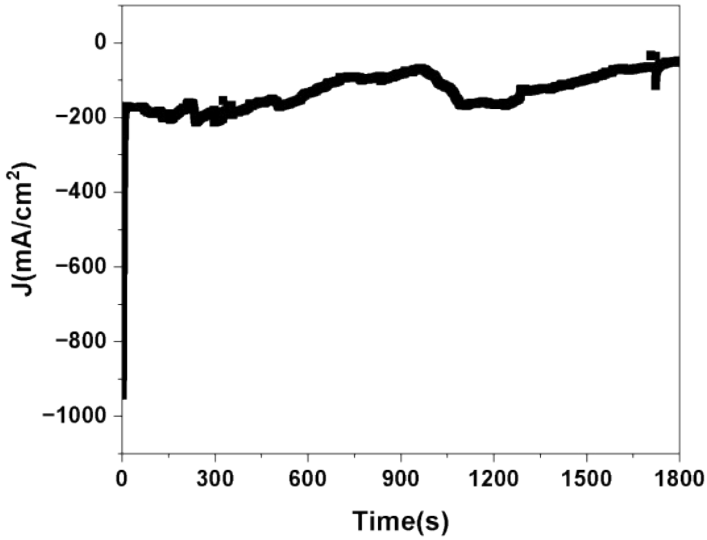

Figure S12. The i-t curve for electrochemical treatment of Cu-$W_{18}O_{49}$-1 in 1 M KOH solution at -0.8 V vs. RHE.

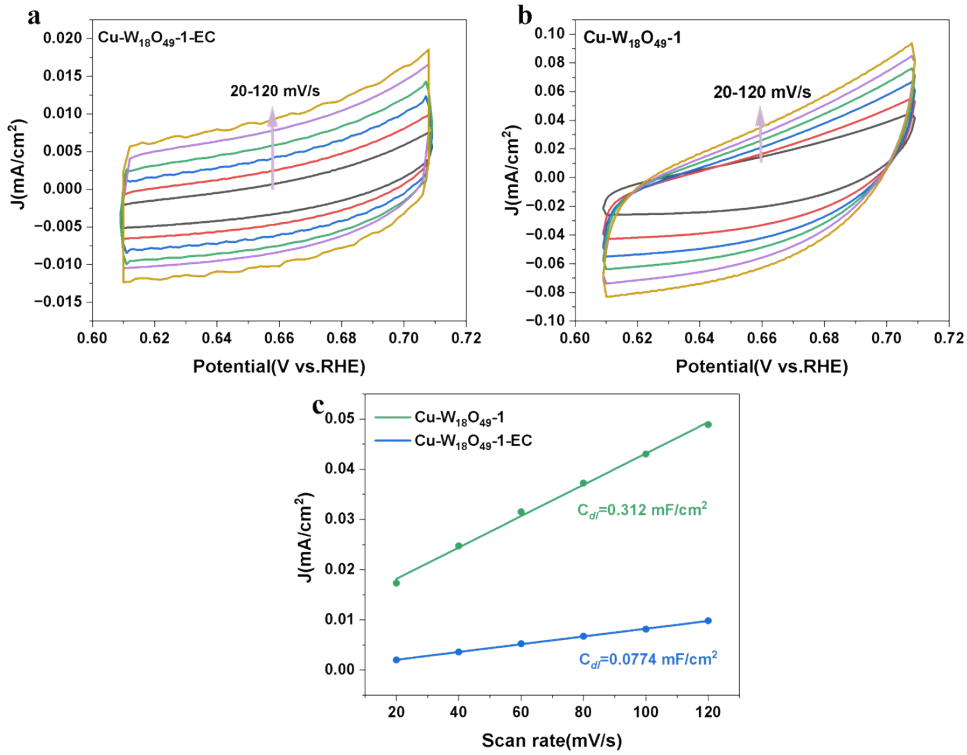

Figure S13. cyclic voltammograms of (a) Cu-$W_{18}O_{49}$-1-EC and (b) Cu-$W_{18}O_{49}$-1 at different scan rates; (c) The double layer capacity values for Cu-$W_{18}O_{49}$-1-EC (blue) and Cu-$W_{18}O_{49}$-1 (green).

Table S5. EDS element analysis of reaction electrode coated by Cu-$W_{18}O_{49}$-1-C and Cu-$W_{18}O_{49}$-1-EC catalysts.

sample	Atomic Conc.(%)		
	Cu	O	W
Cu-$W_{18}O_{49}$-1-C	9.23	26.94	5.11
Cu-$W_{18}O_{49}$-1-EC	19.25	22.91	-

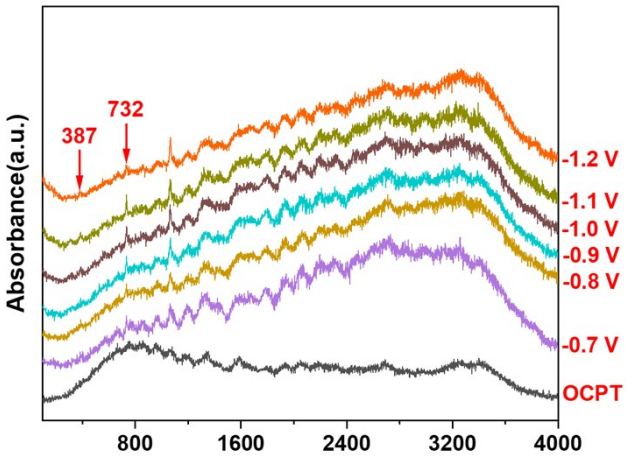

Figure S14. In situ electrochemical Raman spectra of Cu-$W_{18}O_{49}$-0.5 under various applied potentials in 1 M KOH.

References:

1. B. Ravel and M. Newville, ATHENA, ARTEMIS, HEPHAESTUS: data analysis for X-ray absorption spectroscopy using IFEFFIT, *Journal of Synchrotron Radiation*, 2005, **12**, 537–541.
2. J. J. Rehr and R. C. Albers, Theoretical approaches to x-ray absorption fine structure, *Reviews of Modern Physics*, 2000, **72**, 621–654.
3. C. Peng, G. Luo, J. B. Zhang, M. H. Chen, Z. Q. Wang, T. K. Sham, L. J. Zhang, Y. F. Li and G. F. Zheng, Double sulfur vacancies by lithium tuning enhance CO_2 electroreduction to n-propanol, *Nature Communications*, 2021, **12**.
4. W. Zhu, K. Zhao, S. Liu, M. Liu, F. Peng, P. An, B. Qin, H. Zhou, H. Li and Z. He, Low-overpotential selective reduction of CO_2 to ethanol on electrodeposited Cu Au nanowire arrays, *Journal of Energy Chemistry*, 2019, **37**, 176–182.
5. C. J. Chen, X. P. Yan, S. J. Liu, Y. H. Wu, Q. Wan, X. F. Sun, Q. G. Zhu, H. Z. Liu, J. Ma, L. R. Zheng, H. H. Wu and B. X. Han, Highly Efficient Electroreduction of CO_2 to C_{2+}Alcohols on Heterogeneous Dual Active Sites, *Angewandte Chemie-International Edition*, 2020, **59**, 16459–16464.